Tuning the transport properties of graphene films grown by CVD on SiC(0001): Effect of in situ hydrogenation and annealing

Bilal Jabakhanji, A. Michon, Christophe Consejo, Wilfried Desrat, M. Portail, Antoine Tiberj, Matthieu Paillet, Ahmed Azmi Zahab, F. Cheynis, F. Lafont, et al.

Tuning the transport properties of graphene films grown by CVD on SiC(0001): Effect of *in situ* hydrogenation and annealing

B. Jabakhanji,[1] A. Michon,[2] C. Consejo,[1] W. Desrat,[1] M. Portail,[2] A. Tiberj,[1] M. Paillet,[1] A. Zahab,[1] F. Cheynis,[3] F. Lafont,[4] F. Schopfer,[4] W. Poirier,[4] F. Bertran,[5] P. Le Fèvre,[5] A. Taleb-Ibrahimi,[5] D. Kazazis,[6] W. Escoffier,[7] B. C. Camargo,[8] Y. Kopelevich,[8] J. Camassel,[1] and B. Jouault[1]

[1]*Laboratoire Charles Coulomb, CNRS-Université de Montpellier II, Place Eugène Bataillon, 34095 Montpellier Cedex, France*

[2]*CNRS-CRHEA, rue Bernard Grégory, 06560 Valbonne, France*

[3]*Aix Marseille Université, CNRS, CINaM UMR 7325, 13288 Marseille, France*

[4]*Laboratoire National de Métrologie et d'Essais, 29 avenue Roger Hennequin, 78197 Trappes, France*

[5]*Synchrotron SOLEIL, F-91192 Gif Sur Yvette, France*

[6]*CNRS-Laboratoire de Photonique et de Nanostructures, Route de Nozay, 91460 Marcoussis, France*

[7]*Laboratoire National des Champs Magnétiques Intenses (LNCMI), CNRS-UPR3228, INSA, UJF, UPS, Université de Toulouse, 143 avenue de rangueil, 31400 Toulouse, France*

[8]*Instituto de Física "Gleb Wataghin", Universidade Estadual de Campinas, Unicamp 13083-970, Campinas, São Paulo, Brazil*

(Received 1 July 2013; revised manuscript received 24 October 2013; published 24 February 2014)

The structural, optical, and transport properties of graphene grown by chemical vapor deposition (CVD) of propane under hydrogen on the Si face of SiC substrates have been investigated. We show that little changes in temperature during the growth can trigger the passivation of the SiC surface by hydrogen. Depending on the growth condition, hole or electron doping can be achieved, down to a few 10^{11} cm^{-2}. When the growth temperature is high ($T \approx 1500$–$1550\,^{\circ}$C), we obtain electron-doped graphene monolayers lying on a buffer layer. When the growth temperature is slightly lowered ($T \approx 1450$–$1500\,^{\circ}$C), hole-doped graphene layers are obtained, lying on a hydrogen-passivated SiC surface, as confirmed by the enhancement of the mobility (of the order of 4500 cm^2/Vs) and the persistence of weak localization almost up to room temperature (250 K). The high homogeneity of this graphene allows the observation of the half-integer quantum Hall effect, typical of graphene, at the centimeter scale in the best cases. The influence of the SiC steps on the transport properties is discussed.

DOI: 10.1103/PhysRevB.89.085422 PACS number(s): 81.05.ue, 72.80.Vp

I. INTRODUCTION

One of the most promising techniques to produce graphene at the industrial level is silicon sublimation of a silicon carbide (SiC) wafer. In this way, homogeneous epitaxial graphene layers have been obtained on the silicon face of SiC substrates, but the graphene resides on top of the so-called buffer layer or zero layer graphene (ZLG). The ZLG is a $(6\sqrt{3} \times 6\sqrt{3})R30$ reconstructed graphene-like honeycomb lattice with covalent bonds between some of its carbon atoms and the underlying silicon ones. The presence of the ZLG leads to low mobility and high electron concentration in the upper monolayer graphene (MLG). To overcome this problem, various approaches have been developed to dissociate the graphene film from the substrate. The most successful one is postgrowth hydrogen intercalation [1], which drastically decreases the carrier concentration and increases the mobility [2,3]. Because of the reduced interaction with the substrate, MLG on the H-passivated SiC surface has been called "quasifreestanding monolayer graphene" (QFMLG) [1].

As an alternative to SiC sublimation, it has also been shown that graphene can be grown on SiC from an external carbon source [4,5]. Such a direct growth process presents several advantages with respect to the sublimation method. First, a lower growth temperature can be used to grow graphene on 3C-SiC templates on silicon [6] or nanoribbons on textured surfaces [7]. Second, the use of an external carbon supply [6,8] allows one to grow graphene on nonconventional substrates such as sapphire [9]. Concerning SiC, demonstration of the direct growth of graphene on SiC(0001) has been done mainly under ultrahigh-vacuum conditions by molecular beam epitaxy [4,5] (MBE) or by chemical vapor deposition (CVD) with argon as carrier gas [6,9,10] (Ar-CVD). An interesting point to outline is that in spite of the different carbon supply mechanisms, graphene films obtained by MBE or Ar-CVD appear similar to those obtained by the sublimation method. Particularly, both processes lead to the formation of a ZLG on the Si face.

Graphene has also been grown by CVD on SiC using either pure hydrogen or hydrogen/argon mixtures as carrier gas [8,11]. In this case, the presence of hydrogen during the growth has a strong influence on the carbon supply mechanism and the graphene properties. For instance, graphene presents different features on the Si face such as the $(6\sqrt{3} \times 6\sqrt{3})R30$ interface reconstruction (hereafter called $6R3$) or less conventional in-plane rotational disorder [12]. This last feature, more generally observed on the C face when using the sublimation method, is surprising. In an earlier work, the formation of in-plane rotational disorder on the Si face of SiC when using hydrogen as a carrier gas has been attributed to the presence of hydrogen at the graphene/SiC interface, the absence of hydrogen leading to the formation of the $6R3$ interface [8,11]. More recently, additional work suggested that hydrogenation of the substrate may also appear even if the typical $6R3$ reconstruction is detected by low energy electron diffraction (LEED) [12]. In this work, we present a detailed study of graphene films grown by CVD, using mixtures of argon and hydrogen as carrier gas (H/Ar-CVD). The results of angle-resolved photoemission spectroscopy (ARPES) measurements, before and after UHV

annealing, validate clearly the *in situ* hydrogenation of the graphene/SiC interface during the growth. We show that H/Ar-CVD allows one to grow either standard epitaxial graphene or quasifreestanding graphene [3], depending closely on the growth conditions. The key parameters are the growth temperature and the admixture of argon and hydrogen. Remarkably, a small elevation of the growth temperature (∼50 °C) allows changing the nature of the graphene film from QFMLG to MLG on a $6R3$ interface. For the sake of clarity, we will use the terminology HT-MLG, LT-MLG, and IT-FLG for the three samples investigated in this work. HT, IT, and LT refer to high (1550 °C), intermediate (1500 °C), and low (1450 °C) growth temperature, and FLG refers to few layer graphene.

We also investigate the overall homogeneity of the samples, which is a key point for electrical investigations and applications, by performing Raman and magnetotransport measurements. We present two samples with a well defined half-integer quantum Hall effect (QHE). The QHE was observed in the HT-MLG sample at the centimeter scale, which is a unusual result of practical interest. Indeed, the observation of QHE in very large Hall bars is crucial for electrical resistance standards, which are based on precise resistance measurements of the quantum Hall plateaus. The half-integer QHE in epitaxial graphene was measured by several groups [13–17], even with a metrological precision [18], but the size of the devices was systematically less than the millimeter. At the centimeter scale, QHE was only demonstrated with graphene films grown on metals [19].

The paper is organized as follows. In Sec. II, we present the sample growth and characterization techniques. In Sec. III, we present the results obtained on the HT-MLG sample. AFM, Raman, ARPES, and LEED are successively considered. Similarly, Sec. IV presents the results obtained with the IT-FLG and LT-MLG samples. The last part is a discussion before the final conclusion.

II. EXPERIMENTAL DETAILS

Graphene was grown on the Si face of 6H-SiC substrates [8]. The substrates were semi-insulating 0.16° off-axis 6H-SiC wafers purchased from TankeBlue. We used a horizontal hot-wall CVD reactor with propane as the carbon source and hydrogen/argon mixtures as carrier gas [11]. The pressure was 800 mbar and the temperatures ranged from 1450 to 1550 °C. The process began with a temperature ramp followed by a 5 minutes plateau at growth temperature. Then, a 5 cc propane flow was added to the carrier gas, for 1 to 5 minutes. The process ended with a rapid cooling down to room temperature. We summarize in Table I the growth conditions used for the three different samples presented in this work.

Raman spectra were recorded using a home-made setup in which an Acton spectrometer was fitted with a Pylon CCD detector and a 600 grooves/mm grating. The samples were excited with a 532 nm (2.33 eV) continuous wave frequency doubled Nd:Yag laser through a ×100 objective (numerical aperture 0.9). The full width at half maximum of the focused laser spot was ∼400 nm. ARPES measurements were carried out on the Cassiopée beamline at the synchrotron radiation facility SOLEIL. The beamline was equipped with a Scienta R4000 electron analyzer with a ±15° acceptance angle. A photon energy of 36 eV was used with a p polarization and the spectra were collected around the $\bar{K}$ point of the Brillouin zone. Magnetotransport measurements were done in He-pumped cryostats, with pulsed or constant magnetic fields.

TABLE I. Growth parameters used for the three samples investigated in this work: sample names, growth temperatures, proportions of argon and hydrogen in the carrier gas, time during which the propane was added to the carrier gas. The last column indicates the nature of the samples as determined from the measurements. QFFLG refers to quasifree few layer graphene.

sample name	T (°C)	% H	% Ar	t (min)	type
HT-MLG	1550	23	77	5	MLG on ZLG
IT-FLG	1500	23	77	5	QFFLG
LT-MLG	1450	28	72	1	QFMLG

III. HT-MLG: A MONOLAYER GRAPHENE ON ZLG

A. Structural investigation

Figure 1 summarizes the results collected by AFM on the high-temperature sample HT-MLG. Figure 1(a) shows

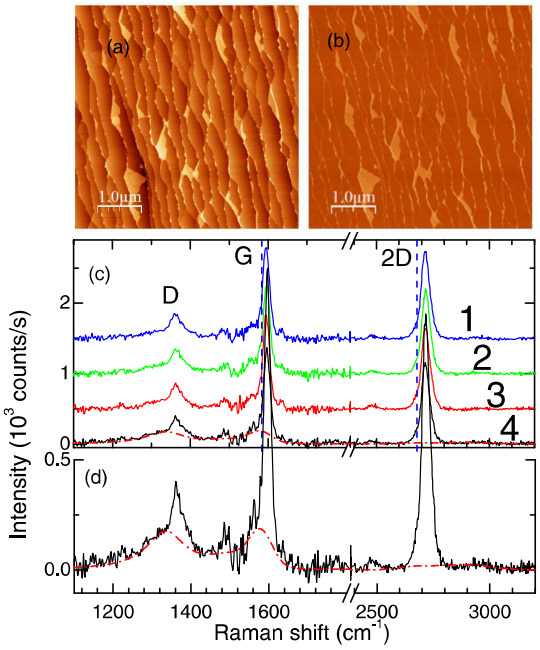

FIG. 1. (Color online) AFM cartography and Raman spectra for sample HT-MLG. (a) SiC terraces are revealed by AFM topography image. (b) The AFM phase image shows no phase contrast, with the exception of the thickest regions. Image dimensions are 5 μm × 5 μm. (c) Raman spectra collected at four different places, with a 532 nm wavelength excitation. All four spectra are identical within the resolution range. The Lorentzian 2D peak and the normalized intensity of the G peak are typical of monolayer graphene. (d) Enlargement of the Raman data at position 4 (black line), and modelization of the Raman signature of the ZLG (red dashed line), taken from Ref. [20]. The good agreement between these two curves suggests the presence of ZLG.

an AFM topography image and Fig. 1(b) the corresponding phase shift. SiC steps are clearly visible in the topography, with typical width 200 nm and height ∼0.7 nm. Small higher parts, close to the SiC step edges, are also visible as white patches. They have an additional height of 0.3 nm. The same regions are also observable in the phase image, as white regions with an additional phase shift of ∼1°. As these regions are higher and close to the step edges, we identify them as small patches with one additional graphene layer on top. The rest of the sample, which covers 90% of the surface observed by AFM, corresponds to a uniform graphene monolayer, as demonstrated below by Raman spectroscopy. Figure 1(c) shows four typical Raman spectra collected at four different positions. The G peak systematically appears at 1595 cm^{-1} with a full width at half maximum (FWHM) ∼20 cm^{-1}. At the millimeter scale, this confirms the excellent homogeneity noticed by AFM. Also, the integrated intensity of the G peak (normalized by the intensity of a reference graphite sample) is about 0.03, which indicates that the average graphene thickness is 1–2 graphene monolayers. The 2D peaks can also be fitted by a single Lorentzian peak centered at 2715 cm^{-1} with a FWHM of 40 cm^{-1}. This shape being incompatible with a Bernal bilayer [21], but consistent with the observation of a single-layer graphene [21], we conclude that the sample is a monolayer graphene [22], with the exception of the small patches of bilayer graphene noticed by AFM. Finally, all spectra in Fig. 1 show a large D peak (∼1350 cm^{-1}) associated with a large broadening at the base of the G peak. This suggests the presence of a ZLG [20,23]. A confirmation can be found in the work of Tiberj *et al.* [20] who analyzed the Raman spectrum of a ZLG on the Si face of a SiC substrate. They proposed a fit, which is reproduced in Fig. 1(c). This fit reproduces quite well the large bases of the experimental D and G peaks, as well as a small peak observed at ∼2900 cm^{-1}, possibly a $D + D'$ peak. From these results, we conclude that, with the exception of small thicker regions at the step edges, the surface is covered by a uniform graphene monolayer on top of a $6R3$ ZLG.

To confirm the nature of the sample, we performed LEED and ARPES measurements, which are reported in Fig. 2. Panel (c) shows a LEED image obtained on the sample, after a moderate annealing at 500 °C. Spots corresponding to SiC, graphene and $6R3$ ZLG are clearly visible. ARPES measurements obtained right after the LEED investigations are shown in panel (a). The linear band structure of monolayer graphene is evidenced. The initial position of the Dirac point at 0.5 eV below the Fermi energy indicates a strong n-type doping ($n \approx 10^{13}$ cm^{-2}). All these results are very similar to those obtained by sublimation of SiC without hydrogenation. A small difference is that there is also a weaker band with a maximum at ∼0.1 eV below the Fermi energy, which we attribute to graphene bilayer patches at the edges of the SiC steps previously evidenced by AFM in Fig. 1. This weak structure disappears after annealing at 1050 °C, where only the well known conical dispersion of MLG is observed, see Fig. 2, panel (b), while no significant changes can be found in the LEED patterns, see panel (d). Si-H bonds should be broken at temperatures above 700 °C [24]; in our case, the disappearance of the bilayer signature at temperatures above 910 °C reveals a partial hydrogenation of the SiC surface. This hydrogenation is only effective below the bilayers. At 1050 °C, the full hydrogen desorption transforms these bilayers into monolayers on ZLG. This scenario implies a relatively high temperature for hydrogen desorption under bilayer graphene, which is in agreement with experimental findings for sample IT-FLG, presented in Sec. IV.

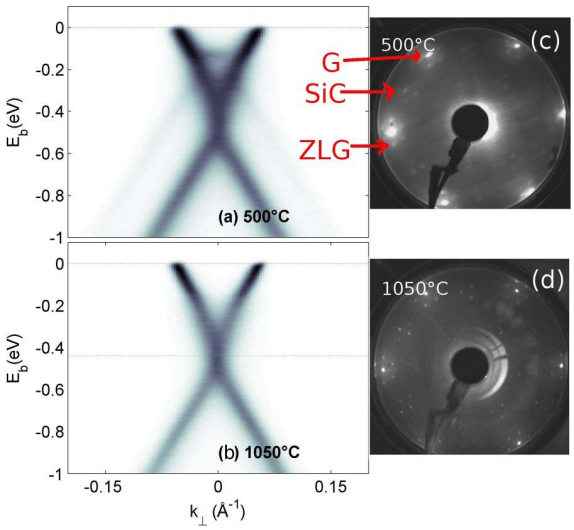

FIG. 2. (Color online) ARPES spectra taken at the $\bar{K}$ point of the graphene Brillouin zone for the HT-MLG sample presented in Fig. 2 after (a) initial outgassing at 500 °C and (b) annealing at 1050 °C. The spectra were acquired along the direction perpendicular to the $\Gamma\bar{K}$ direction in reciprocal space. The photon energy was 36 eV. The light was p polarized. The reference of the binding energy E_b is the Fermi energy E_F, indicated by a red dotted line. In (b), the binding energy at the Dirac point is indicated by a dotted green line. The corresponding LEED images measured at 70 eV after initial outgassing at 500 °C and annealing at 1050 °C are also presented in (c) and (d), respectively.

B. QHE at the centimeter scale

To assess the quality of MLG, magnetotransport measurements were performed on several parts of the HT-MLG sample. We label $R_{//}$ and $R_{\perp}$ the van der Pauw configurations which correspond to the current source connected parallel and perpendicular to the substrate steps, respectively. Before the annealings at 500 °C and above, when only a mild heating at 150 °C is done before the measurements, the electrical anisotropy $R_{\perp}/R_{//}$ is about 4 and there is a strong n-type doping ($n \sim 6.5 \times 10^{12}$ cm^{-2}) with a low carrier mobility (400 cm^2/Vs). This electron concentration, which is very close to the one deduced from ARPES measurements, can be drastically reduced by adequate preparation. For instance, we outgassed a 6 mm × 6 mm square of this HT-MLG sample for 60 min at 300 °C under vacuum in a furnace a few hours before the measurements. Then we put it in a wet atmosphere [25] (90% humidity) for two days before the measurements at low temperature. Figures 3(c)–3(e) show different resistances at $T = 1.7$ K: $R_{\perp} = R_{23,14}$, $R_{//} = R_{43,12}$, and the Hall resistance $R_H = R_{13,42}$. Here, $R_{ab,cd}$ corresponds to a resistance measured between contacts c and d when current is injected between contacts a and b, and the connections are sketched in Fig. 3(a). With respect to unprepared samples, the electron concentration decreases by an order of magnitude,

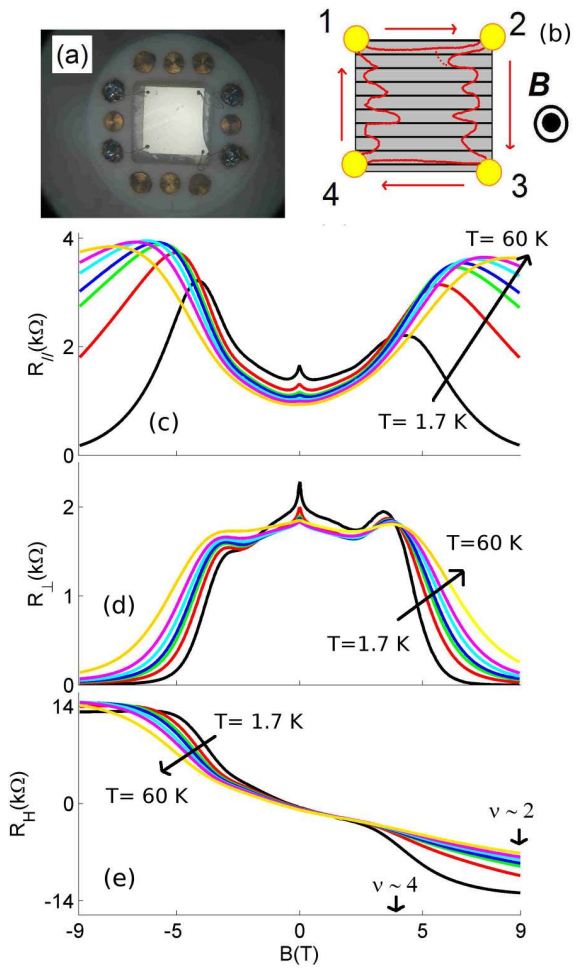

FIG. 3. (Color online) (a) Top view of a 6 mm × 6 mm sample HT-MLG. (b) Sketch of the sample connections, with respect to the SiC steps. Contacts are indicated by yellow circles, edge states by a red solid line, SiC steps by horizontal lines. Edge state scattering (dashed red line) is sketched in the vicinity of contact 2. (c), (d), (e) Magnetoresistances $R_{//}(B) = R_{43,12}$, $R_{\perp} = R_{23,14}$, and $R_H = R_{13,42}$, respectively, taken at various temperatures: $T =$ 1.6, 7, 15, 20, 30, 40, and 60 K.

down to ∼4–5 × 10^{11} cm^{-2}, and the mobility increases up to 1600 cm^2/Vs. Note that this low electron concentration is not intrinsic, and is reversible. The samples retrieve their high electron concentration when they are left a few days under vacuum.

The half-integer quantum Hall effect is evidenced in the Hall resistance at low temperature ($T \sim 1.7$ K). The plateaus at $\sim \pm R_K/2$ (where $R_K = h/e^2$) are associated with a cancellation of the longitudinal resistance in $R_{\perp}(B)$, while $R_{//}$ also strongly decreases. The $R_H(B)$ curve is somehow asymmetric in B, as R_H also includes a longitudinal component. Both the anisotropy revealed by $R_{//}$ and $R_{\perp}$ at high field and the positive magnetoresistance of $R_{//}$ at low field suggest a relation to the stepped surface structure. Other works have focused on anisotropic quantum Hall effect in epitaxial graphene obtained by sublimation [15], where the anisotropy and positive magnetoresistance (for a configuration equivalent

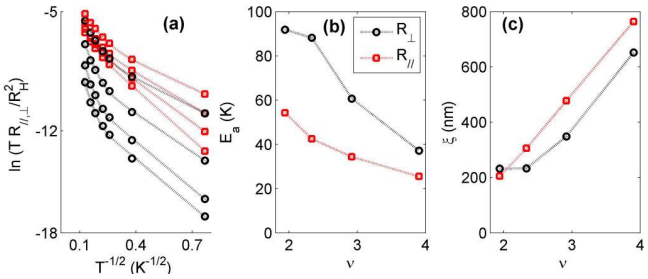

FIG. 4. (Color online) (a) Plots of $TR_{\perp}/R_H^2$ (black curves) and $TR_{///}/R_H^2$ (red curves) as a function of $T^{-1/2}$ at $B = 4.4$, 6, 7.5, and 9 T (top to bottom). Open circles and squares are experimental data, dashed lines are theoretical fits. Two parameters of the fits, the activation energy E_a and the localization length ξ, are reported in (b) and (c) as a function of the filling factor ν.

to $R_{\perp}$) were finally attributed to backscattering of edge states by the SiC steps. In our case, the positive magnetoresistance predominantly affects $R_{//}$. We believe this to be purely incidental, as similar measurements, performed on another HT-MLG sample, have shown a large magnetoresistance on $R_{\perp}$ and not $R_{//}$ (see also Fig. 7 for sample IT-FLG). Scattering between edge states in the vicinity of the contacts, as depicted in Fig. 3(b), is probably at play. Besides, the anisotropy at $B = 0$ ($R_{//} < R_{\perp}$) is systematically observed in all samples and can be more clearly attributed to the SiC steps.

The temperature dependance of the magnetoresistance can be satisfactorily fitted by a model which takes into account a mixing of variable range hopping (VRH), effective at low temperature ($T < 20$ K), with thermal activation [26], important at higher T. The data and the fits are reported in Fig. 4, panel (a). Details of the calculation can be found in the Appendix. From the fits were extracted an activation energy E_a in panel (b) and a localization length ξ in panel (c), as a function of the filling factor ν. An important disorder is evidenced by the low activation energies shown in panel (b). The activation energy is roughly ten times smaller than the theoretical value $v_F\sqrt{2\hbar eB}/2$, where v_F is the Fermi velocity, indicating Landau level broadening due to disorder. The anisotropy of the activation energy strongly suggests that the source of disorder is linked to the SiC steps. The largest values of ξ are observed at the center of a Landau level, when ν comes close to 4, as expected. ξ is then comparable to the average SiC step width and, instead of diverging, seems to saturate. This last point needs additional measurements, but is in agreement with results presented in Sec. IV on sample LT-MLG.

To conclude this part, we have shown that standard MLG can be grown by Ar/H CVD on SiC(0001) using a moderate mixture of hydrogen and argon as carrier gas. Provided the growth temperature is high enough to break all H bonds at the surface of the SiC wafer faster than the formation of the graphene, no modification of the $6R3$ ZLG appears. All graphene properties are identical to the ones of sublimation graphene, with similar n-type doping and limited mobility. The only advantage, inherent to the CVD deposition process, is a sufficient homogeneity to observe the QHE on samples at the centimeter scale. To go a step further, it is necessary to

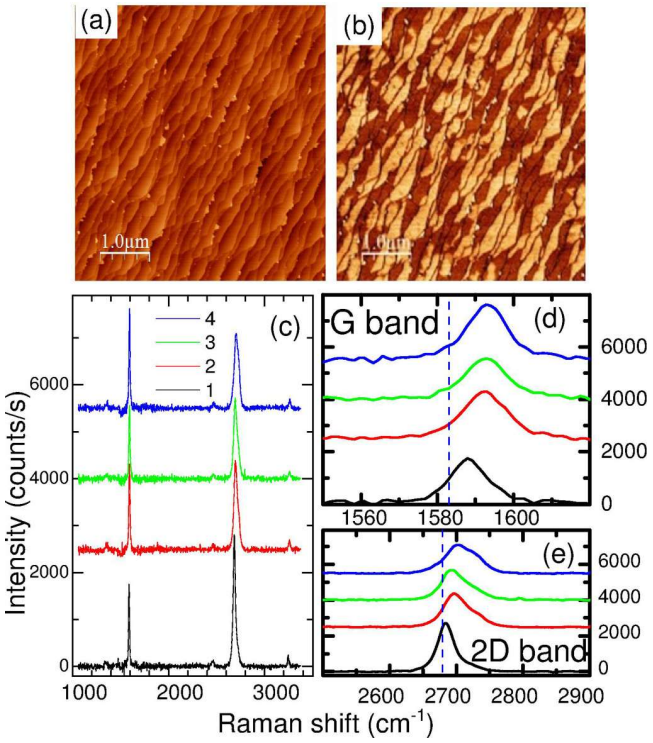

FIG. 5. (Color online) AFM cartography for IT-FLG. (a) SiC terraces are revealed by a 5 μm $\times$ 5 μm AFM topography image. (b) The corresponding AFM phase is bimodal, with a 1° phase shift between the two modes. The phase difference is evidenced by white and dark regions. Regions with a phase shift of +1° are indicated in white. (c) Raman spectra at four different spots for sample IT-FLG. (d) The positions of the G peaks differ, but the normalized intensities of the G peaks are typical of graphene monolayer-bilayer. (e) The 2D bands have several components and differ from place to place. The overall shape of the band is not compatible with homogeneous graphene monolayer or bilayer. However, in relation with the AFM phase, it can be interpreted as a spatial averaging of monolayer and bilayer areas.

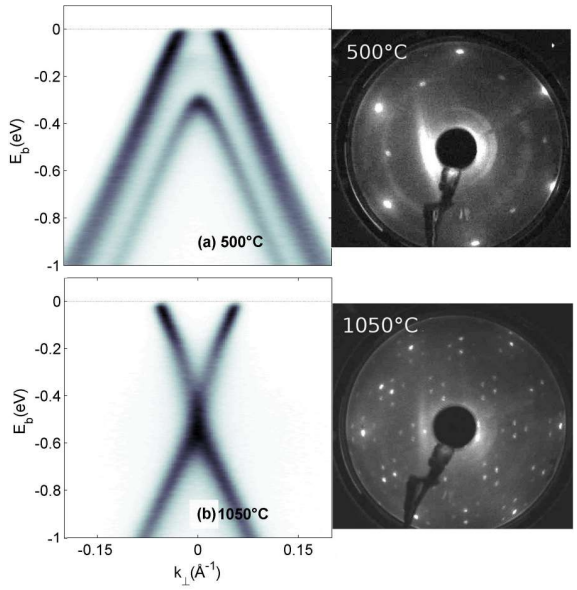

FIG. 6. (Color online) ARPES spectra taken at the $\bar{K}$ point of the graphene Brillouin zone for sample IT-FLG after (a) initial outgassing at 500 °C, (b) annealing 1050 °C. LEED images measured at 70 eV after each annealing are also indicated.

lower the desorption rate during the growth, i.e., to lower the temperature.

IV. INCREASING THE HYDROGENATION LEVEL

Reducing the growth temperature by 50 °C results in a completely different sample, named IT-FLG. Figure 5 shows results collected by AFM mapping. Figure 5(a) shows the topography of a 5 μm $\times$ 5 μm region of the sample. Figure 5(b) shows the corresponding phase image. It is clearly bimodal, some regions appearing white, some others appearing dark. The phase difference is about +1° for the white regions. This AFM phase image obviously brings new information with respect to the AFM topography, because the phase is sensitive to the mechanical and dissipative properties of the observed surface. Similar observations have already been reported in the literature [27,28]. Bolen *et al.* have found a phase difference of 1°–2° between ZLG and graphene [27]. Hibino *et al.* [28] have found that on annealed 4H-SiC(0001), areas of different numbers of graphene layers can be clearly discriminated in the AFM phase image. The situation is similar in this work, with compelling evidences by Raman (Fig. 5), ARPES, and LEED (Fig. 6) that the whole SiC surface has been hydrogen passivated, with an admixture of monolayer and Bernal bilayer graphene on top. As in Fig. 1, we attribute the regions with higher (white) phase to Bernal graphene bilayer, and the regions with lower (dark brown) phase to MLG.

Figures 5(c)–5(e) show Raman spectra collected at four different positions, separated by more than 1 mm. Figures 5(d) and 5(e) show enlargements of the Raman spectra presented in Fig. 5(c), focusing on the G and $2D$ bands, respectively. The integrated intensity of the G peak, normalized by the intensity of a reference graphite sample, is about 0.03–0.04, which indicates that the sample is either a monolayer, a bilayer, or a mix of mono- and bilayer. The $2D$ peak is asymmetric for all positions reported in Fig. 5(e) but the asymmetry varies from one position to another. The complex shape of the $2D$ peak is attributed to the averaging of graphene mono- and bilayers under the Raman spot, whose diameter (400 nm) is comparable to the sizes of the mono- and bilayer regions in Fig. 5(b). These two areas cannot be attributed to a bare ZLG, because in this case a much broader and intense D peak would be observed [20,23].

The *in situ* hydrogenation of IT-FLG is evidenced in Fig. 6 by ARPES measurements around the $\bar{K}$ point of the graphene Brillouin zone. For the sample outgassed at 500 °C, a complex band structure is found; see panel (a). This band structure is a superimposition of band structures for graphene mono- and bilayers, which are both heavily p doped. The bands of monolayers and the low-energy bands of the bilayers almost coincide in Fig. 6(a), but in ARPES spectra taken slightly outside the Dirac point ($k_{//} > 0$, where $k_{//}$ is along

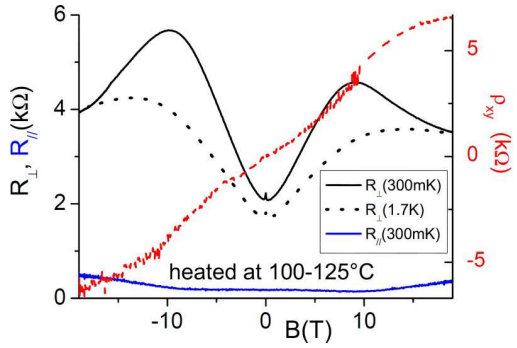

FIG. 7. (Color online) Magnetoresistances of sample IT-FLG. Black and blue lines: van der Pauw resistances $R_\perp$, $R_{//}$ at 300 mK; dashed black line: $R_\perp$ at 1.7 K; the transverse resistivity $\rho_{xy}(B)$ (red dotted line), calculated as the asymmetric part of the Hall resistance, shows the trace of quantum plateaus at ∼6 kΩ, as expected for graphene bilayer.

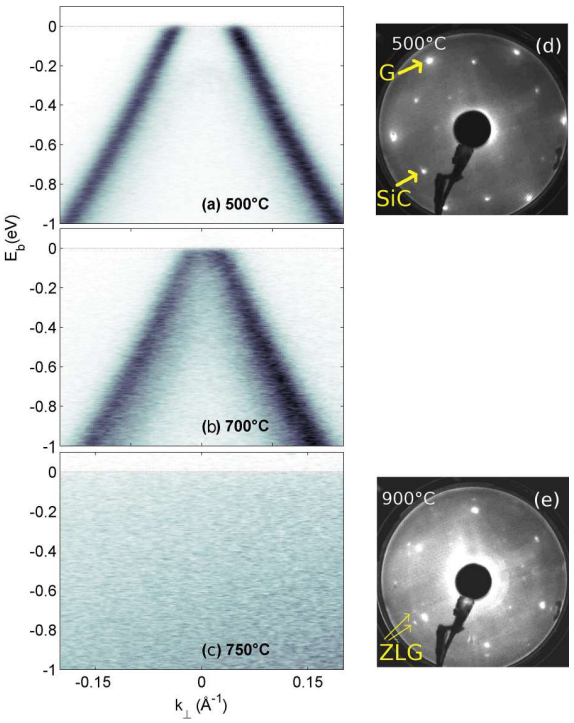

FIG. 8. (Color online) ARPES spectra taken at the $\bar{K}$ point of the graphene Brillouin zone for hydrogenated sample LT-MLG after (a) initial outgassing at 500 °C, (b) annealing at (b) 700 °C, (c) 750 °C. (d) and (e) LEED images measured at 70 eV after the annealings at 500 °C and 900 °C. Yellow labels G, SiC, and ZLG point to the spots corresponding to graphene, SiC, and the ZLG, respectively.

the $\Gamma\bar{K}$ direction), the bands for mono- and bilayers can be distinguished separately.

To check the stability of the hydrogenation process we performed successive annealings under UHV. A first annealing at 730 °C first reduces the p doping. The following annealing at 810 °C transforms the initially p-doped sample into an n-doped sample. After annealing at 930 °C, the MLG band structure completely disappears, and only the BLG structure remains. Finally, after the final annealing at 1050 °C, the single MLG band structure is retrieved, which indicates that hydrogen has now completely desorbed; see panel (b).

The formation of a ZLG is also evidenced by the LEED patterns, presented in Fig. 6. It is only after annealings at temperatures higher than 930 °C than the spots of the $6R3$ reconstructed ZLG become visible.

Before the annealings at 500 °C and above, the magnetoresistances of the sample IT-FLG have been measured and are reported in Fig. 7. With respect to ARPES measurements, the hole concentration is reduced to $p \sim 1.6 \times 10^{12}$ cm^{-2} by a simple heating at 100 °C under vacuum. We attribute the changes in carrier concentration to desorption of molecular species, like water or oxygen, but this point would deserve more detailed studies. The mobility is about 1200 cm^2/Vs. Because of the low concentration, the quantum regime is reached at moderate magnetic fields, as confirmed by pronounced dips observed in $R_\perp$ at $B \sim 10$ T. Also, the transverse resistivity $\rho_{xy} \approx [R_H(B) - R_H(-B)]/2$ shows onsets of plateaus at ∼±6 kΩ, confirming that the sample has some of the electrical characteristics of a graphene bilayer. However, the large B-symmetric component remaining in the Hall resistance $R_H(B)$ confirms the inhomogeneous nature of the sample.

To summarize, all structural characterizations show that lowering the temperature by 50 °C from 1500 to 1450 °C results in a hydrogenation of the substrate, but the graphene of the sample IT-FLG is inhomogeneous. Therefore, a third sample was grown with a few growth adjustments, at a slightly reduced temperature of 1450 °C; see Table I. This resulted in a pure monolayer of graphene on top of a hydrogenated substrate, as evidenced in Fig. 8. After a first outgassing at 500 °C, a linear band structure is found in ARPES measurements; see panel (a). This band structure corresponds to monolayer graphene, heavily p-type doped ($p \sim 6 \times 10^{12}$ cm^{-2}). The following annealings up to 700 °C reduce the p-type doping to 10^{12} cm^{-2}; see panel (b). After annealing at 750 °C, the band structure of the monolayer completely disappears; see panel (c). This behavior is closely similar to the one already observed in Ref. [1]. Consequently, we attribute the disappearance of the monolayer band structure to hydrogen desorption, with formation of a ZLG.

This progressive formation of the ZLG is even better evidenced from the LEED patterns, collected at two stages of the annealings; see panels (d) and (e). After the initial outgassing at 500 °C, the graphene and SiC spots are clearly visible, but no spots corresponding to a $6R3$ ZLG are visible. The situation remains unchanged up to annealings above 750 °C or above, where the spots corresponding to the $6R3$ ZLG become visible, while the spots corresponding to the original graphene layer become very weak.

We also performed magnetotransport at low temperature, before the annealings. The anisotropy is $R_\perp/R_{//} \sim 2$, the mobility 4800 cm^2/Vs and 4400 cm^2/Vs at $T = 1.5$ K and 300 K, respectively, and the carrier concentration $p = 7.6 \times 10^{12}$ cm^{-2} varies by less than one percent between 1.5 and 300 K. The carrier concentration extracted from the Hall coefficient is in agreement with ARPES measurements. The mobility is obviously higher than in HT-MLG samples, and decreases by only 10% between 1.5 and 300 K. A part of this sample was processed in large Hall bar devices (100 μm width,

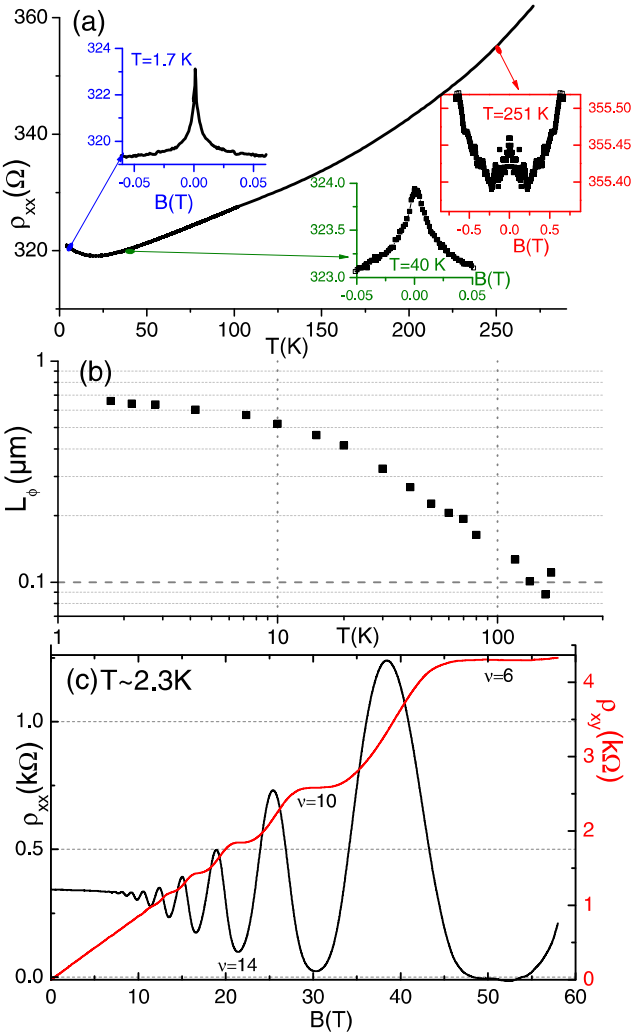

FIG. 9. (Color online) (a) Temperature dependence of the resistivity of sample LT-MLG, from $T = 1.7$ K up to 290 K. The insets show the magnetoresistance induced by weak localization at $T = 1.7$ K and 250 K. (b) Coherence length as a function of temperature, extracted from fits of the weak localization peak. (c) Magnetoresistances at low temperature ($T = 2.3$ K) up to $B = 58$ T, revealing the half-integer quantum Hall effect. The measurements have been performed with Hall bars of width 100 μm and length 500 μm. The graphene was covered by PMMA.

500 μm long) and covered by PMMA for additional protection. Figure 9(a) shows the resistivity of one of these Hall bars, as a function of T. The weak temperature dependence is typical of QFMLG. Also, the persistence of a weak localization peak almost up to room temperature (250 K) indicates a rather weak scattering by the remote phonons of the substrate. From the fit of the weak localization, we extract the coherence length L_ϕ, which is plotted in Fig. 9(b) as a function of T. L_ϕ exceeds the width of the SiC steps at low temperature, which confirms the carpet-like nature of the graphene film over the SiC steps. In Fig. 9(c) the magnetoresistivities of the Hall bar up to $B = 58$ T unambiguously show Shubnikov–de Haas oscillations and half-integer QHE typical of graphene, confirming the spatial homogeneity of the graphene film and

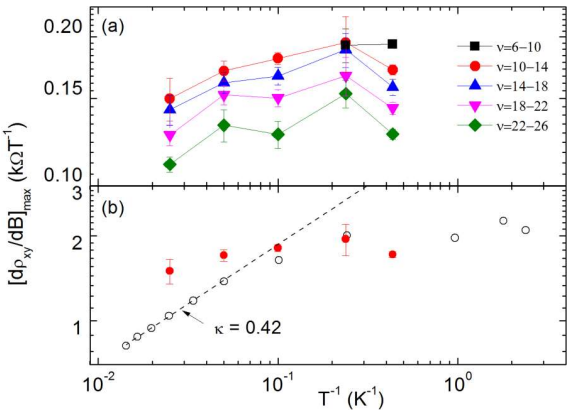

FIG. 10. (Color online) (a) $(d\rho_{xy}/dB)_{\max}$ vs $1/T$ measured from 2.3 to 40 K. Numbers correspond to filling factors of adjacent quantum Hall plateaus. (b) Open symbols correspond to the data of Fig. 5 from Ref. [29], and dashed line is fit to the function $T^{-\kappa}$ with $\kappa = 0.42$. $(d\rho_{xy}/dB)_{\max}$ data points obtained for our graphene sample multiplied by factor 10 are given by solid symbols and related to the transition between $\nu = 10$ and $\nu = 14$ quantum Hall plateaus.

of its carrier density. Plateaus corresponding to filling factor $\nu = 6, 10, 14, 18, 22, 26$ are visible.

In order to gain more insight on structural disorder effects on electron transport in this sample, we measured QHE at various temperatures and analyze the transitions between adjacent quantum Hall (QH) plateaus. According to the scaling theory, the maximum slope of the Hall resistivity step $(d\rho_{xy}/dB)_{\max}$ and the half width of the $d\rho_{xx}/dB$ peak scale as $T^{-\kappa}$ with $\kappa \sim 0.42$ [30]. To verify this predicted scaling behavior, we plotted in Fig. 10(a) the maximum slope $(d\rho_{xy}/dB)_{\max}$ vs $1/T$ for various plateau-plateau transitions. The obtained exponent $\kappa = 0.1 \pm 0.02$ is far too small as compared to the value $\kappa \sim 0.4$ measured for graphitic [29,31,32] and many other QH systems. It is still too small even if compared with $\kappa \sim 0.2$ observed in some spin-degenerate QH systems [33,34]. However, as Fig. 10(b) illustrates, the apparent low value of κ has a simple explanation that results from the saturation of $\kappa(T)$ at low enough temperatures. The saturation behavior has been identified to be a finite-size effect when the quantum phase coherence length $L_\phi(T)$ reaches the sample size or other characteristic scale at the saturation temperature T_s [32,35]. Seemingly, in our graphene sample, $T_s \geqslant 40$ K. According to Fig. 9(b), $L_\phi(40\text{ K}) \sim 0.25$ μm, suggesting that the cutoff length is much smaller than the sample size (100 μm) and can be naturally associated with the stripe or terrace width originating from the steplike structure of epitaxial graphene.

V. DISCUSSION AND CONCLUSION

From these results we have demonstrated that the nature of graphene grown by CVD under argon and hydrogen, on the Si face of SiC substrate, is strongly similar to graphene obtained by SiC sublimation, with or without postgrowth hydrogenation. In fact, no clear differences could be evidenced between these sublimated and CVD graphene, as far as LEED, ARPES, Raman, and transport are concerned. We also determined the experimental conditions which are necessary

for the hydrogenation process to take place during the CVD growth. When the growth temperature is high ($T \geqslant 1550\,^{\circ}$C), the samples are homogeneous graphene monolayers, n doped, on top of a ZLG. When the growth temperature is slightly decreased ($T \leqslant 1500\,^{\circ}$C), no ZLG can be found by LEED and Raman anymore and samples are p doped. In this last case, hydrogenation of the SiC substrate seems obvious, when our results are compared with other results gathered by other groups on graphene obtained by sublimation with postgrowth hydrogenation. Finally, because of the good spatial homogeneity, we were able to report the observation of the half-integer quantum Hall effect for both types of samples. Remarkably, for n-doped samples, the quantum Hall effect can even be evidenced directly at the centimeter scale. This is encouraging with respect to the potential of the material for applications in electronics.

ACKNOWLEDGMENTS

We thank M. George, J.-R. Huntzinger, S. Contreras, and C. Glattli for enlightening discussions. This work was partly supported by the French Agence Nationale de la Recherche (Grant No. ANR-2011-NANO-004-06), and by the European Union (Project PodiTrodi-EU No. FP7 287770). Part of this work has been performed at LNCMI-Toulouse and is supported by EuroMagNET, Contract No. 228043. We acknowledge support by CNPq and FAPESP.

APPENDIX

In the quantum Hall regime, on the magnetic field ranges which correspond to the Hall plateaus, the conductivity is given by the Efros-Shlovskii variable range hopping (VRH) regime:

$$\sigma_{xx} \propto \frac{T_0}{T} \exp(-\sqrt{T_0/T}), \tag{A1}$$

where the temperature T_0 is given by

$$k_B T_0 = Ce^2/4\pi\epsilon\epsilon_0\xi \tag{A2}$$

and ξ is the localization length; $C \sim 6.2$ is a numerical constant [36]. It was recently observed, in graphene samples, that VRH can be extended far into the regions of plateau transitions [26], as predicted by the model of Polyakov and Shklovskii [37]. We assume that it is also the case here. Then, still following Ref. [26], the data at high temperatures ($T > 15$ K) are better fitted by including an activation energy E_a and the conductivity is given by

$$T\sigma_{xx} = \alpha \exp(-\sqrt{T_0/T}) + \beta T \exp(E_a/k_B T), \tag{A3}$$

where α and β are additional parameters which correspond to the relative influence of thermal activation and VRH. Because of the strong anisotropy, the conductivities in the direction parallel and perpendicular to the steps have been approximated by $R_{//}/R_H^2$ and $R_{\perp}/R_H^2$, respectively, and fitted separately. We also tested a fit of the averaged conductivity, which gives similar results to those presented in Fig. 4. The filling factor is approximated by $\nu = n_s h/eB$ and n_s is chosen by pinning $\nu = 4$ at $B = 4.3$ T, where a maximum is detected in $R_{\perp}$ and $R_{//}$ at low temperature. Nevertheless, in view of the experimental data, an additional variation of n_s with B is possible.

[1] C. Riedl, C. Coletti, T. Iwasaki, A. A. Zakharov, and U. Starke, Phys. Rev. Lett. **103**, 246804 (2009).
[2] S. Forti, K. V. Emtsev, C. Coletti, A. A. Zakharov, C. Riedl, and U. Starke, Phys. Rev. B **84**, 125449 (2011).
[3] F. Speck, J. Jobst, F. Fromm, M. Ostler, D. Waldmann, M. Hundhausen, H. B. Weber, and T. Seyller, Appl. Phys. Lett. **99**, 122106 (2011).
[4] A. Al-Temimy, C. Riedl, and U. Starke, Appl. Phys. Lett. **95**, 231907 (2009).
[5] E. Moreau, F. J. Ferrer, D. Vignaud, S. Godey, and X. Wallart, Phys. Status Solidi A **207**, 300 (2010).
[6] M. Portail, A. Michon, S. Vézian, D. Lefebvre, S. Chenot, E. Roudon, M. Zielinski, T. Chassagne, A. Tiberj, J. Camassel, *et al.*, J. Cryst. Growth **349**, 27 (2012).
[7] T. Kajiwara, Y. Nakamori, A. Visikovskiy, T. Iimori, F. Komori, K. Nakatsuji, K. Mase, and S. Tanaka, Phys. Rev. B **87**, 121407 (2013).
[8] A. Michon, S. Vézian, A. Ouerghi, M. Zielinski, T. Chassagne, and M. Portail, Appl. Phys. Lett. **97**, 171909 (2010).
[9] J. Hwang, V. Shields, C. Thomas, S. Shivaraman, D. Hao, M. Kim, A. Woll, G. Tompa, and M. Spencer, J. Cryst. Growth **312**, 3219 (2010).
[10] W. Strupinski, K. Grodecki, A. Wysmolek, R. Stepniewski, T. Szkopek, P. E. Gaskell, A. Grüneis, D. Haberer, R. Bozek, J. Krupka *et al.*, Nano Lett. **11**, 1786 (2011).
[11] A. Michon, L. Largeau, A. Tiberj, J. R. Huntzinger, O. Mauguin, S. Vézian, D. Lefebvre, F. Cheynis, F. Leroy, P. Müller *et al.*, Mater. Sci. Forum **740–742**, 117 (2013).
[12] A. Michon, S. Vézian, E. Roudon, D. Lefebvre, M. Zielinski, T. Chassagne, and M. Portail, J. Appl. Phys. **113**, 203501 (2013).
[13] T. Shen, J. J. Gu, M. Xu, Y. Q. Wu, M. L. Bolen, M. A. Capano, L. W. Engel, and P. D. Ye, Appl. Phys. Lett. **95**, 172105 (2009).
[14] X. Wu, Y. Hu, M. Ruan, N. K. Madiomanana, J. Hankinson, M. Sprinkle, C. Berger, and W. A. de Heer, Appl. Phys. Lett. **95**, 223108 (2009).
[15] T. Schumann, K.-J. Friedland, M. H. Oliveira, A. Tahraoui, J. M. J. Lopes, and H. Riechert, Phys. Rev. B **85**, 235402 (2012).
[16] T. J. B. M. Janssen, A. Tzalenchuk, R. Yakimova, S. Kubatkin, S. Lara-Avila, S. Kopylov, and V. I. Fal'ko, Phys. Rev. B **83**, 233402 (2011).
[17] B. Jouault, N. Camara, B. Jabakhanji, A. Caboni, C. Consejo, P. Godignon, D. K. Maude, and J. Camassel, Appl. Phys. Lett. **100**, 052102 (2012).
[18] T. J. B. M. Janssen, J. M. Williams, N. E. Fletcher, R. Goebel, A. Tzalenchuk, R. Yakimova, S. Lara-Avila, S. Kubatkin, and V. I. Fal'ko, Metrologia **49**, 294 (2012).
[19] T. Shen, W. Wu, Q. Yu, C. A. Richter, R. Elmquist, D. Newell, and Y. P. Chen, Appl. Phys. Lett. **99**, 232110 (2011).
[20] A. Tiberj, J.-R. Huntzinger, N. Camara, P. Godignon, and J. Camassel, arXiv:1212.1196.

[21] A. C. Ferrari, J. C. Meyer, V. Scardaci, C. Casiraghi, M. Lazzeri, F. Mauri, S. Piscanec, D. Jiang, K. S. Novoselov, S. Roth *et al.*, Phys. Rev. Lett. **97**, 187401 (2006).
[22] N. Camara, J.-R. Huntzinger, G. Rius, A. Tiberj, N. Mestres, F. Pérez-Murano, P. Godignon, and J. Camassel, Phys. Rev. B **80**, 125410 (2009).
[23] F. Fromm, M. H. Oliveira Jr., A. Molina-Sánchez, M. Hundhausen, J. M. J. Lopes, H. Riechert, L. Wirtz, and T. Seyller, New J. Phys. **15**, 043031 (2013).
[24] N. Sieber, T. Seyller, L. Ley, D. James, J. D. Riley, R. C. G. Leckey, and M. Polcik, Phys. Rev. B **67**, 205304 (2003).
[25] T. O. Wehling, A. I. Lichtenstein, and M. I. Katsnelson, Appl. Phys. Lett. **93**, 202110 (2008).
[26] K. Bennaceur, P. Jacques, F. Portier, P. Roche, and D. C. Glattli, Phys. Rev. B **86**, 085433 (2012).
[27] M. L. Bolen, S. E. Harrison, L. B. Biedermann, and M. A. Capano, Phys. Rev. B **80**, 115433 (2009).
[28] H. Hibino, H. Kageshima, and M. Nagase, J. Phys. D **43**, 374005 (2010).
[29] T. Shen, A. T. Neal, M. L. Bolen, J. J. Gu, L. W. Engel, M. A. Capano, and P. D. Ye, J. Appl. Phys. **111**, 013716 (2012).
[30] H. P. Wei, D. C. Tsui, M. A. Paalanen, and A. M. M. Pruisken, Phys. Rev. Lett. **61**, 1294 (1988).
[31] Y. Kopelevich, J. H. S. Torres, R. R. da Silva, F. Mrowka, H. Kempa, and P. Esquinazi, Phys. Rev. Lett. **90**, 156402 (2003).
[32] A. J. M. Giesbers, U. Zeitler, L. A. Ponomarenko, R. Yang, K. S. Novoselov, A. K. Geim, and J. C. Maan, Phys. Rev. B **80**, 241411 (2009).
[33] S. W. Hwang, H. P. Wei, L. W. Engel, D. C. Tsui, and A. M. M. Pruisken, Phys. Rev. B **48**, 11416 (1993).
[34] E. Pallecchi, M. Ridene, D. Kazazis, F. Lafont, F. Schopfer, W. Poirier, M. O. Goerbig, D. Mailly, and A. Ouerghi, Sci. Rep. **3**, 1791 (2013).
[35] W. Li, C. L. Vicente, J. S. Xia, W. Pan, D. C. Tsui, L. N. Pfeiffer, and K. W. West, Phys. Rev. Lett. **102**, 216801 (2009).
[36] A. Efros, N. V. Lien, and B. Shklovskii, Solid State Commun. **32**, 851 (1979).
[37] D. G. Polyakov and B. I. Shklovskii, Phys. Rev. Lett. **70**, 3796 (1993).